

MODEL-BASED OPTIMIZATION OF THE SWITCHING PERFORMANCE OF A SWITCH DISCONNECTOR

R. CHECHARE^a, CH. RÜMPLER^{b,*}, A. MUJAWAR^a, K. BEDNARSKI^c

^a Eaton India Innovation Center, Pune, Maharashtra 411028, India

^b Eaton Industries GmbH, 53115 Bonn, Germany

^c Eaton Electrical Products Limited, LE12 5TH Leicestershire, United Kingdom

* ChristianRuempler@Eaton.com

Abstract. Low voltage switch disconnectors (SD) combine rated load switching with disconnector functionality, providing safe electrical isolation. Electrical contacts are separated forming an arc discharge that needs to be quenched at first current zero (CZ) to protect the load and the SD itself. With increased line voltage, interruption at first CZ crossing is getting more difficult due to increased transient recovery voltage (TRV) and larger post arc current, leading to excessive contact erosion with longer arcing time. Arc simulation methodology was utilized to improve the design for better arc cooling close to CZ. Therefore, benchmark values of arc resistance and thermal time constant were evaluated close to CZ for a successful test at lower line voltage. The cooling efficiency of different designs at higher line voltage was analyzed by 3D arc simulation. A revised design was able to clear overload currents at lower and higher line voltages at first CZ, preventing excessive contact damage.

Keywords: Switch disconnector, arc discharge, arc simulation, model driven development.

1. Introduction

Low voltage (LV) switch disconnectors (SD) are manually operated mechanical switching devices for rated current AC or DC switching, providing safe electrical isolation from the circuit. Further functionality is a true OFF position indication for the main contacts and prevention of unintended re-closing of the contacts. Overload and short circuit protection are provided by upstream devices such as molded case circuit breakers (MCCB) or fuses. Switch disconnectors are sometimes used for direct switching of electric machines. Due to inrush effects, the currents may rise up to 8-12 times of the rated current of the switch disconnector. Even with these high currents exceeding the rated current multiple times, the magnetic force generated by the current path is not strong enough to effectively elongate and pull the arc as in a current limiting circuit breaker. Therefore, the arc remains on the main contacts until current zero (CZ) crossing appears, and the arc is extinguished ideally at the first CZ. Depending on the effectiveness of the arc cooling before and after the CZ crossing, multiple current half cycles might be needed to achieve current interruption. With multiple current half cycles, heavy erosion of the main contacts is likely leading to issues such as high contact resistance, no continuity, contact welding, or complete destruction of the contact system.

In this contribution, a systematic design approach using numerical modeling is described to overcome these challenges, leading to a SD design that can interrupt overload currents within the first half cycle. This approach is applied to speed up the arc chamber development, reducing the number of design cycles

and development tests. Furthermore, modeling provides insights into physical processes during switching inside the arc chamber that are not easy to obtain experimentally.

1.1. Load cases

A low voltage switch disconnector for AC applications needs to pass overload certification test as per IEC60947-1, IEC60947-3, and UL98 standards [1–3]. These tests have stringent requirements on the number of making and breaking operations, followed by a temperature rise test. The SD rated currents and voltages are 160 A/415 V, 100 A/690 V, and 100 A/600 V respectively. Three load cases are considered for concept verification tests:

- IEC 415 V/1280 A (8x rated current),
- IEC 690 V/800 A (8x rated current), and
- UL 600 V/600 A (6x rated current).

1.2. Challenges due to increased line voltage

The switch disconnector design under investigation is a CZ interruption device. Increasing the line voltage does increase the challenges to achieve current interruption at CZ, as the transient recovery voltage (TRV) is increasing too. To withstand the voltage, plasma has to cool down rapidly in order to prevent a substantial post arc current flow and to regain dielectric strength in the contact gap. Better arc cooling helps to increase the arc resistance, required for CZ interruption at higher line voltage load cases, ideally preventing multiple half cycles of current flow. But with insufficient arc cooling, multiple half cycles could occur, especially in the tests that require multiple make

and break operations. Additionally, temperature rise tests done after overload tests can become challenging due to increased contact resistance. Therefore, it is important to achieve interruption at CZ crossing after first half cycle to improve contact life.

1.3. Paper organization

The arc simulation approach used to perform the design optimization of the new SD and the evaluation criteria for the arc cooling efficiency are described in section 2. In section 3, the initial SD design is analyzed for the 415 V line voltage load case to quantify the arc cooling characteristics. As this design was tested successfully at this load case, arc resistance and thermal time constant values are used as a base-line when comparing model results for increased line voltage load cases and design optimization. Results indicate the need for improved arc cooling for increased line voltage load cases. Several design changes are investigated in section 4 to improve the arc cooling close to CZ, quantified and compared with benchmark load case and initial design. Verification test results for low and increased line voltage load cases are presented in section 5, followed by conclusions in section 6.

2. Model approach

2.1. Arc simulation

The simulation of the arcing phenomena during switching is performed with a magneto-hydrodynamics (MHD) approach, describing the arc as a thermal plasma [4]. Arcing in an electrical device is complex physical phenomenon as it involves multiple physical processes such as electromagnetics, fluid flow, heat transfer, evaporation, condensation, and erosion. Governing equations for fluid flow (Navier-Stokes) and electromagnetic fields (Maxwell) are solved using a partitioned coupled approach [5]. Fluid flow and heat transfer equations are solved in ANSYS® Fluent [6] using finite volume methods. Electric and magnetic equations are solved using in-house solver with finite elements method. Transfer of fields from one solver to another is achieved with the help of the coupling tool OCoS [7], as shown in figure 1. The model accounts for the erosion of metal mass in liquid and vapor state as well as ablation of plastics [8]. Built-in parallel capabilities of the solvers are used to reduce the turnaround time of the solution.

2.2. Quantification of arc cooling efficiency

The evaluation of the cooling efficiency in this contribution is based on the theory of the dynamic arc, developed by Mayr and Cassie [9] and described by equations (1) and (2)

$$\frac{1}{g_m} \frac{dg_m}{dt} = \frac{1}{\tau_m} \left[\frac{u_b i}{P_0} - 1 \right] \quad (1)$$

$$\frac{1}{g_c} \frac{dg_c}{dt} = \frac{1}{\tau_c} \left[\frac{u_b^2}{u_{b0}^2} - 1 \right]. \quad (2)$$

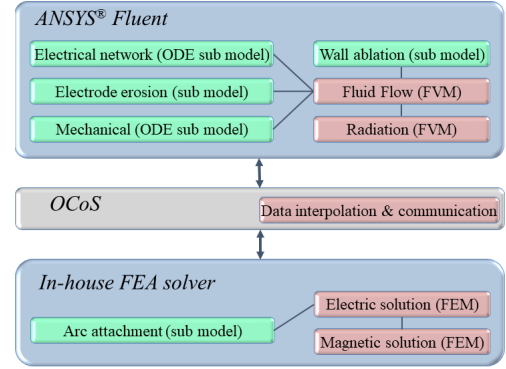


Figure 1. Arc simulation framework.

Here g_m and g_c are the arc conductance, i is the current, τ_m and τ_c are the thermal time constants for the arc decay, u_b is the arc voltage, u_{b0} is the constant fraction of the arc voltage, and P_0 is the cooling power.

Equation (1) can be used to describe the dynamic arc behavior of a low current arc with conduction losses only, whereas equation (2) can be applied to describe the dynamic behavior of a high current arc with axial convection losses. In our case, the conditions are not that clearly separable, as the main flow component is crossing the arc while venting through the venting ports close to CZ. We do not try to identify the parameters needed in these equations, but use the arc resistance and time constants, evaluated just before CZ, to quantify the effectiveness of the arc cooling. A fast decaying arc plasma results in a quick decrease of the electrical conductivity and hence, fast rising arc resistance. A time constant τ (without a suffix, as we do not specify which cooling method is more dominant) is calculated and a smaller value indicates faster arc cooling, thus rapid increase in arc resistance. Therefore, higher values of arc resistance and lower values of time constant indicates an improved possibility to interrupt the current at the first CZ crossing and thus lower the possibility of multiple half cycles. The method applied here is simplistic and not a replacement for a more sophisticated analysis of post arc current (thermal restrike) and dielectric recovery, but it can be seen that the method is leading to useful predictions and design decisions. This type of black-box modeling is mostly applied in high-voltage (HV) and medium-voltage (MV) applications. However, such an approach can also provide useful results in LV applications, as described in [10], where the authors applied black-box modeling for the interruption of a 7.2–9.2 kA currents with 480 V and 500 V circuits. In a time interval of 50 μ s before CZ, the time constant for Mayr's equation yields 1.06 μ s and for post CZ, the time constant yields 76 μ s. Even though the designs and conditions in [10] are quite different from the device under investigation here, some order of magnitude estimates are helpful to evaluate new SD results.

3. Initial design analysis

3.1. Switch disconnecter design

The baseline design of the new SD (OFF position) is shown in figure 2, where main components are labeled: moving contact, fixed contact, terminal, and contact bridge. This is a double break design, with two contacts in series. When the SD knob is turned by an operator, the contact bridge starts moving and contacts are separated, initiating an arc discharge (arc on each one of contact pairs). Cold air and hot plasma that is present in the arc chamber escapes through the venting area to the surroundings. As discussed in the introduction, the current should be cleared quickly to reduce the damage of contacts due to excessive erosion, and to protect the load. Interruption is achieved when a re-ignition of the arc after CZ is avoided by a fast plasma recovery. The initial design of the new SD was

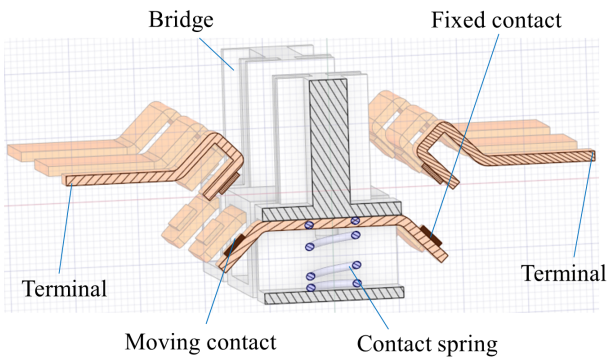


Figure 2. Initial design of the switch disconnecter.

first successfully tested at a lower line voltage load case 415 V/1280 A first. The results indicate sufficient arc cooling, as the interruption was successful at first CZ crossing. Therefore, the 415 V/1280 A load case is considered as the benchmark when comparing arc cooling characteristics with increased line voltage load cases.

To get benchmark values, arc simulation is performed for this 415 V/1280 A load case to quantify arc resistance and arc time constant just before the CZ crossing. The same baseline design was then analyzed applying increased line voltage load cases 690 V/800 A and 600 V/600 A, to compare the arc cooling characteristics with those from benchmark case.

3.2. Modeling approach

Only one pole of SD is modeled, using a symmetry plane at the center of the pole. Computational fluid dynamics (CFD) and finite element analysis (FEA) meshes for different contact arm positions are prepared upfront and the motion of the contact is modeled, as described in [11]. For the initial contact position, CFD mesh and FEA mesh consist of 258k and 443k cells respectively, with average element size of 0.5 mm. The prepared meshes are used to replace the meshes on the fly during the transient simulation run, corresponding

to the contact arm position. A multi body dynamics (MBD) model was used to calculate the contact motion upfront, providing a position vs. time profile that is used to control the dynamic mesh in the arc model. The contact travels 5.9 mm distance in 3 ms upon opening by the bridge. During the opening of electromechanical contacts, the arc is immobile for a few ms, depending on: contact speed, contact material, the current, and the magnetic field driving the arc. Since there is no self-consistent model available for this phenomenon, the arc immobility time of 2 ms is estimated and considered in MHD simulations [12]. Metal vapor erosion from contacts is calculated by two mechanism, a rate-based and an energy-based approach. The rate-based erosion mechanism represents the metal evaporation at microscopic anode and cathode spots, proportional to the charge. Thus, a constant erosion rate is applied (kg/As) [5]. The energy-based erosion mechanism is representing the mass loss in the macroscopic arc spot due to melting and evaporation of the electrode material at a larger spot area. Therefore the heat transfer into the electrodes as well as phase change processes (melting, vaporization) are calculated by means of a separate 1D finite-volume solver. The 1D heat transfer solver is also supporting the calculation of the plastic ablation mass sources from the surrounding walls [8]. The sheath voltage drop at the arc root is modeled using a non-linear resistance in the FEA model [5]. The simulation is carried out for one half cycle until the first CZ crossing is reached and the arc cooling characteristics can be evaluated. An explicit time discretization scheme is used for the CFD solution, thus the time step size is adjusted by the solver in each iteration so that the Courant number does not exceed a value of one. The time step size close to CZ is about $3 \cdot 10^{-8}$ s, to provide an example.

3.3. Results and discussion

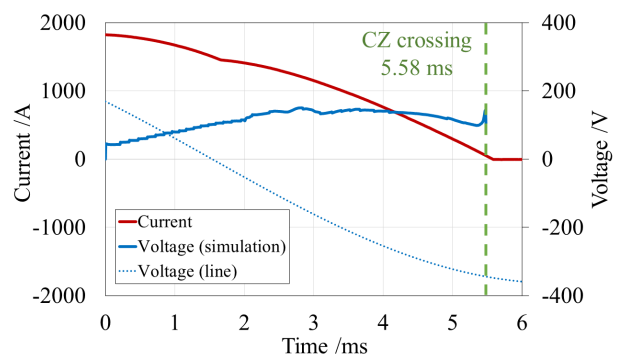


Figure 3. Simulation result for 415V/1280A load case (initial design).

The calculated arc voltage for the 415 V/1280 A load case is shown in figure 3. As indicated in the figure, the time point of CZ crossing in this case is $t=5.58$ ms. To observe the dynamic arc behavior close to CZ, figure 4 shows the arc resistance in a short 50 μ s time

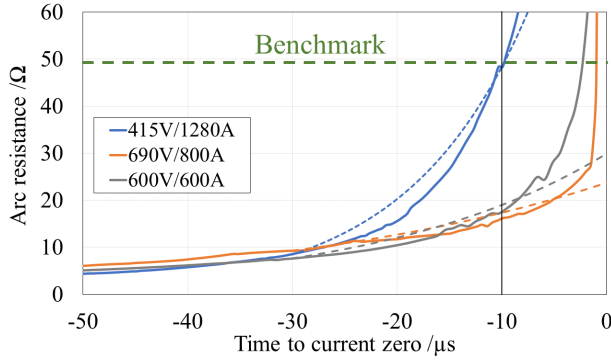


Figure 4. Arc resistance variation just before CZ crossing (initial design). Solid lines represent the model results, dashed lines show the exponential curve fit according to (3).

interval before reaching CZ. This plot enables also the comparison of simulation results with the other load cases simulated with the same set of meshes, since all curves show the same short time interval before CZ. The arc resistance value R_{10} , evaluated at $t=10\ \mu\text{s}$ before CZ crossing, is considered as the benchmark value to compare the arc cooling efficiency for the different load cases. Sophisticated modeling of the post arc current after CZ crossing was not done, but further metrics of arc cooling can be derived fitting the arc resistance curve to an exponential function. In our data analysis, we use an exponential growth fit according to

$$R(t) = R_{30} \cdot e^{\frac{t}{\tau}} . \quad (3)$$

Here τ is the time constant and R_{30} is the starting arc resistance value for the fit, extracted at $30\ \mu\text{s}$ before CZ. The time constant τ is adjusted to provide some reasonable fit from $30\ \mu\text{s}$ up to $10\ \mu\text{s}$ before CZ. Calculated values closer to CZ are questionable, since the arc is shrinking rapidly and it is questionable if the mesh resolution still sufficient. Additionally, deviation from local thermodynamic equilibrium (LTE) can be expected close to CZ, which is not represented by the model.

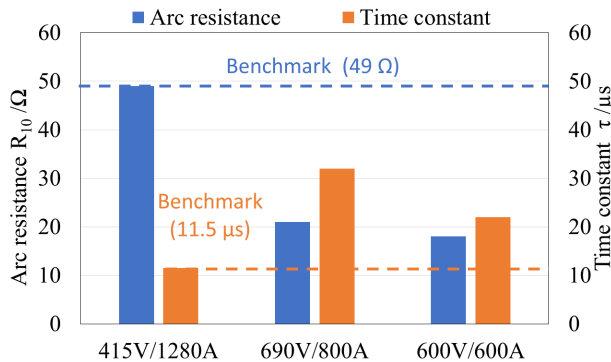


Figure 5. Comparison of arc resistance R_{10} and time constant τ for different load cases (initial design).

In case of the $415\ \text{V}/1280\ \text{A}$ load case, an arc resistance of $49\ \Omega$ and a time constant of $\tau=11.5\ \mu\text{s}$ is

calculated, quantifying the arc cooling characteristics. These values are considered as benchmark values when comparing with increased line voltage load cases. Figure 4 shows the transient behavior of the arc resistance just before CZ for the other load cases with higher line voltage too. In comparison to the benchmark case, the rate of rise of the arc resistance and the R_{10} value of the arc resistance are much lower. Figure 5 provides a comparison of the values with the benchmark, showing a significant increase of the arc time constant for the $690\ \text{V}/800\ \text{A}$ and $600\ \text{V}/600\ \text{A}$ load cases, as well as substantially lower R_{10} arc resistance values. The arc cooling is insufficient in these cases, increasing the risk of multiple half cycles of current flow when switching higher line voltage load cases.

This risk was verified by performing a $690\ \text{V}/800\ \text{A}$ prototype test, as shown in figure 6. The arc was not extinguished during multiple half cycles of current flow, until the upstream fuse cleared the fault.

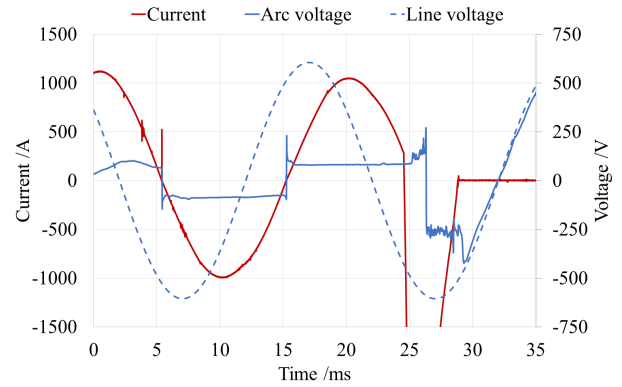


Figure 6. Test result for $690\ \text{V}/800\ \text{A}$ load case (initial design).

Based on these results, several iterations for design improvements need to be devised to enable successful switching of all load cases. To improve the arc cooling, the different heat transfer mechanisms need to be considered: conduction, convection, and radiation.

Close to CZ, convective cooling due to gas flow inside the arc chamber – driven by pressure gradients – is a significant arc cooling mechanism. The lack of cooling in case of the higher line voltage load cases is visualized by means of temperature plots in a cross section (cut plane) between the contacts at CZ, as shown in figure 7. Using the same temperature scale, one can observe the higher arc temperatures as well as larger arc region in case of $690\ \text{V}/800\ \text{A}$ and $600\ \text{V}/600\ \text{A}$ load cases. With temperatures well above $5000\ \text{K}$, the plasma is still conductive, and a post-arc current is flowing leading to a thermal restrike.

The reduced ampacity ($600\ \text{A}/800\ \text{A}$ vs. $1280\ \text{A}$) in case of higher line voltage leads to a reduced arc power in the high current phase of the switching cycle. As arc power and pressure are correlated, pressure built up in the arc chamber is lower in these cases compared to the higher ampacity case. Peak arc power values for $600\ \text{A}$,

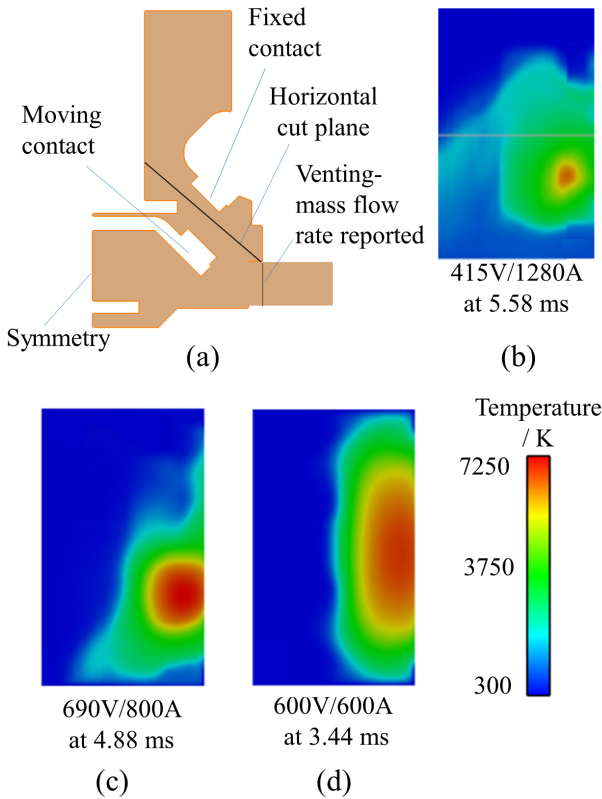


Figure 7. Temperature contours in a cross section between the contacts at CZ crossing: (a) Location of contour plane, (b) 415 V/1280 A, (c) 690 V/800 A, and (d) 600 V/600 A (initial design).

800 A, and 1280 A load cases are 97 kW, 98 kW, and 180 kW, which results in peak pressures of 1.32 bar, 1.38 bar, and 1.97 bar respectively. A reduction of the mass flow leaving the arc chamber through the venting opening prior to CZ crossing is the result, as depicted in figure 9 for the initial design. This is an indicator for a reduction of the convective cooling of the arc, leading to a reduced switching performance.

4. Model-based optimization

4.1. Revised design

In order to improve the arc resistance close to CZ, the effect of multiple geometric variations has been studied through simulations. The venting cross section of the initial design was reduced by a factor of 3.6, reducing the venting mass flow rate during the first half cycle of current flow early in the interruption. As a result, the arc chamber is more pressurized. This improved the mass flow through the venting just before CZ, leading to an improved convective arc cooling. In addition, ferromagnetic plates are introduced to speed up the arc motion, pulling the arc out of the contact gap. Simulations with the revised design were performed for all load cases to quantify and compare the arc cooling characteristics with the benchmark values.

4.2. Results and discussion

The arc resistance is plotted over time for the revised design and all load cases just before CZ crossing in figure 8. In case of the revised design, arc resistance values above or close to the benchmark value at CZ are realized, indicating a better arc cooling compared to the initial design.

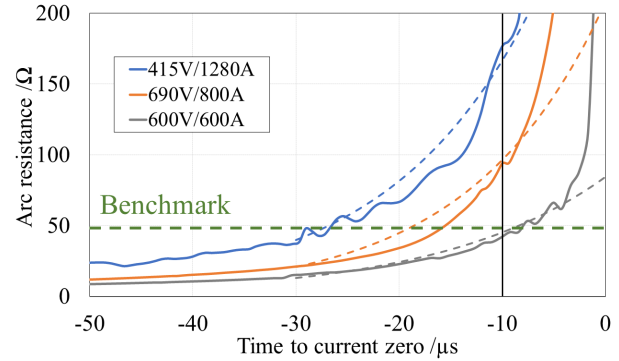


Figure 8. Arc resistance variation just before CZ crossing (revised design). Solid lines represent the model results, dashed lines show the exponential curve fit according to (3).

With the design changes, a major improvement of the mass flow rate leaving the venting port before CZ has been achieved, as shown in figure 9. A substantial increase of the mass flow rate for all load cases could be achieved with the revised design, improving the convective arc cooling.

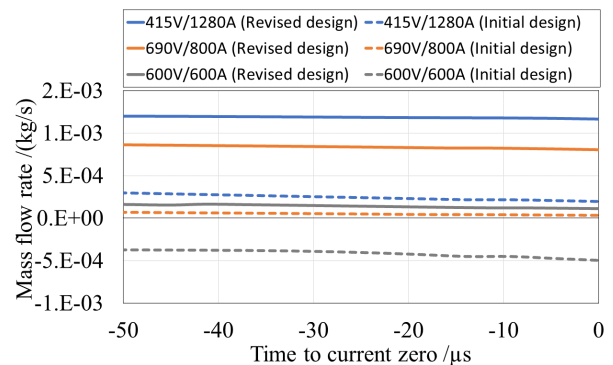


Figure 9. Mass flow rate comparison for the initial and revised designs and different load cases.

The flow conditions in the contact gap for the revised design and the 690 V/800 A load case are visualized in figure 10. Here, contour plots of temperature, overpressure, and flow velocity are shown for two cross section plots. One plane, as shown in figures 10 (a)–(c), is located at the center of the contact (perpendicular to the contact surface). To visualize the venting conditions, the cross section of another set of plots, shown in figures 10 (d)–(f), has a 6.6 mm offset to the first plane, since the center plane does not cut directly through a venting path. Temperature at CZ has been decreased to a maximum value of 4000 K, compared

to more than 7000 K in the original design, see figure 7 (c). With reduced temperature, the electrical conductivity in the contact gap is reduced effectively, preventing a post arc current to establish (thermal restrike). The pressurization of the chamber with 0.25 bar overpressure is leading to venting velocities of 800 m s^{-1} , removing hot gas effectively from the chamber.

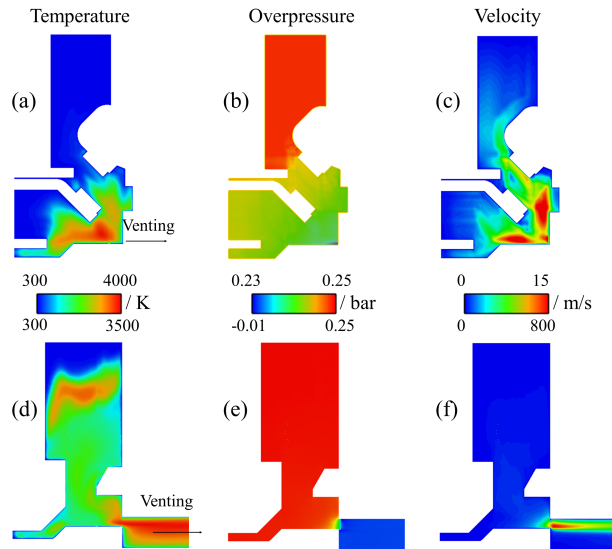


Figure 10. Temperature, overpressure, and flow velocity contours in two cross sections at CZ crossing for revised design and 690V/800A load case: figures (a)–(c) show a cross section at the center of the contact, figures (d)–(f) a cross section with 6.6mm offset to center of the contact.

The improvement can also be seen in figures 11a and 11b, where a comparison of the arc resistance values R_{10} and R_{30} is shown.

For further quantification of the improved cooling efficiency, time constant values according to equation (3) are shown in figure 11c for the initial and revised design. The time constants achieved with the revised design are not significantly larger than the benchmark value, and a reduction for the 690 V/800 A and 600 V/600 A load cases in comparison to the initial design was achieved. As a better arc cooling leading to faster plasma decay, the possibility of current interruption in the first half cycle is increased and should be achievable with the optimized design based on this analysis.

With the revised design, a 1.5x increase of the R_{10} arc resistance just before CZ could be achieved for the 600 V/600 A load case, getting close to the benchmark value of 49Ω . As this load case was the worst condition in the initial design, it is selected for verification through testing. Due to the reduced venting cross section and increased pressure build up in the arc chamber, the risk of structural failure of the SD housing is increased. As this risk is higher at 415 V/1280 A load case due to higher arc energy, testing at lower voltage and higher current was also

considered for verification through testing.

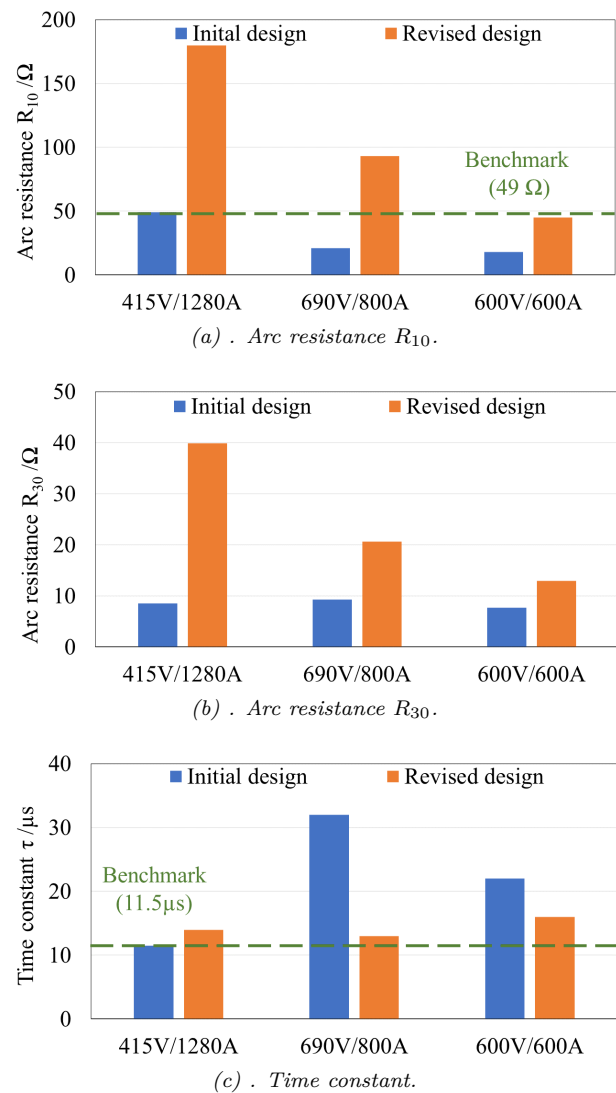


Figure 11. Comparison of initial and revised design comparing calculated arc resistances R_{10} and R_{30} as well as time constants for different load cases.

5. Verification of revised design

Testing was performed for 600 V/600 A load case using two samples. Both tested samples passed the test clearing the current in the first half cycle. The waveforms from one of the samples are shown in figure 12a. These waveforms show current and arc voltage traces starting from the instance when contacts were just separated until the current is switched off. The sample for structural integrity testing was tested at slightly higher line voltage of 525 V and 1280 A current. As shown in figure 12b, current was cleared in the first half cycle, without any issue regarding structural integrity. With these modifications and interruption in the first half cycle, the design passed tests that require multiple SD operations as per the standards.

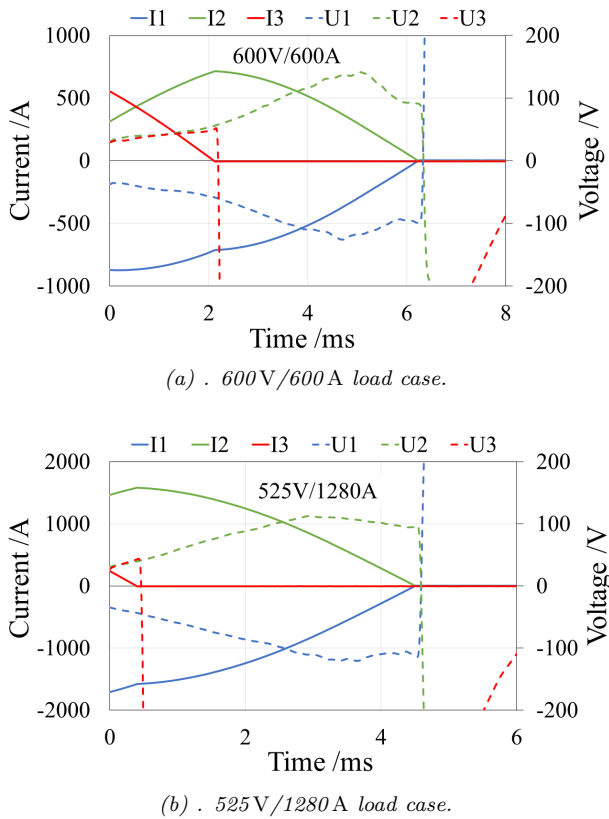


Figure 12. Revised design verification results showing measured current and arc voltage traces for two load cases.

6. Conclusions

Thanks to arc simulation methods, model-based optimization could be performed in the development process of a new switch disconnector design. To establish benchmark data and identify the direction of design optimization, an initial design was investigated which was successfully tested at a lower line voltage load case but failed at higher voltages. Arc resistance and time constant were quantified for the successful lower line voltage case and set as main targets to prevent multiple half-cycles of current flow in cases of higher line voltage cases, as these values quantify the arc cooling efficiency. Simulation results at higher line voltage showed that the initial design had to be improved, as arc cooling was not sufficient. A smaller induced mass flow rate at CZ crossing was identified as a reason, causing reduced convective cooling. The analysis of design changes (reduction of venting area, addition of ferromagnetic plates), which were realized in a revised design, showed an improved arc cooling behavior in comparison to the initial design. The model-based findings for the revised design were verified by testing at 600 V/600 A and 525 V/1280 A load cases. All test samples interrupted the current successfully in the first half cycle, avoiding excessive erosion as in multiple cycle interruption. The structural integrity of the prototypes remain unaffected in all cases.

References

- [1] Low-voltage switchgear and controlgear – Part 1: General rules. IEC Standard 60947-1, The International Electrotechnical Commission, 2020.
- [2] Low-voltage switchgear and controlgear – Part 3: Switch-disconnectors and fuse-combination units. IEC Standard 60947-3, The International Electrotechnical Commission, 2020.
- [3] Standard for safety for enclosed and dead-front switches. UL Standard 98, UL Standards & Engagement, 2016.
- [4] A. Gleizes, J. J. Gonzalez, and P. Freton. Thermal plasma modelling. *Journal of Physics D: Applied Physics*, 38(9):R153–R183, April 2005. doi:10.1088/0022-3727/38/9/R01.
- [5] C. Rümpler. *Lichtbogensimulation für Niederspannungsschaltgeräte*. Dissertation, Technische Universität Ilmenau, 2009.
- [6] ANSYS® Fluent. Release 19.2, ANSYS, Inc., 2018.
- [7] OCoS. Release 2021, Fraunhofer Institute SCAI, Sankt Augustin. URL: <https://www.scai.fraunhofer.de>.
- [8] C. Rümpler, H. Stammberger, and A. Zacharias. Low-voltage arc simulation with out-gassing polymers. In *2011 IEEE 57th Holm Conference on Electrical Contacts (Holm)*, pages 1–8, Sept 2011. doi:10.1109/HOLM.2011.6034770.
- [9] W. Rieder. *Plasma und Lichtbogen*. Friedr. Vieweg & Sohn, 1967.
- [10] A. Balestrero, L. Ghezzi, M. Popov, et al. Black box modeling of low-voltage circuit breakers. *IEEE Transactions on Power Delivery*, 25(4):2481–2488, 2010. doi:10.1109/TPWRD.2010.2047872.
- [11] C. Rümpler and V. R. T. Narayanan. Arc modeling challenges. *Plasma Physics and Technology*, 2(3):261–270, 2015.
- [12] K. Hirose. Immobility phenomena of the DC electric arc of large current driven by magnetic field. *The Journal of the Institute of Electrical Engineers of Japan*, 80:931–940, 1960.